COMITATO NAZIONALE PER L'ENERGIA NUCLEARE
Laboratori Nazionali di Frascati

LNF-73/36
13 Giugno 1973

(Revised Nov. 1973)

R. Barbini, S. Faini, C. Guaraldo, C. Schaerf and R. Scrimaglio : ENERGY LOSS SPECTROMETER FOR LOW ENERGY PION SCATTERING. -

Servizio Documentazione
dei Laboratori Nazionali di Frascati del CNEN
Casella Postale 70 - Frascati (Roma)

Laboratori Nazionali di Frascati del CNEN
Servizio Documentazione

LNF-73/36
13 Giugno 1973

R. Barbini, S. Faini, C. Guaraldo, C. Schaerf and R. Scrimaglio:
ENERGY LOSS SPECTROMETER FOR LOW ENERGY PION SCATTERING. -

ABSTRACT. -

The performance of an energy loss spectrometer is reported together with a detailed discussion of the basic parameters of such a system and in particular the second order aberrations. The system we have constructed consists of two uniform field seventy degree bending sectors in a configuration symmetrical to first order, with an image point in the symmetry plane. The system has been tested with the LEALE-LNF low energy positive and negative pion beams. The magnets were set at zero degrees facing each other. The contributions of the aberrations and of multiple Coulomb scattering in air, Helium and thin windows to the momentum resolution of the two magnets system have been evaluated and the total momentum resolution compared with the experiment at various energies for positive and negative pions.

1. - INTRODUCTION. -

A large amount of information on nuclear structure has been obtained through the elastic and inelastic scattering of high energy particles on nuclei.

Since the nuclear levels are closely spaced, careful measurements of the energy transferred in the target nucleus can be obtained only if the resolution is sufficiently great.

Such resolution has been achieved previously with a highly monochromatic incident beam and a comparable energy resolution of the scattered particles. Unfortunately, the beams from high energy accelerators, i.e. primary and secondary beams, are not very monochromatic. (The energy resolution of the beam accelerated by an electron linac is usually not better than 0.01). For this reason only a small fraction of the produced high energy particles can be used for high resolution scattering experiments thus limiting the useful beam intensity.

In order to overcome this limitation, a different approach was suggested previously[1] to the problem of designing the best magnetic spectrometer for analyzing high energy particles before and after scattering. The significant requirement was not the energies of the incident or scattered particles but the energy difference. This energy lost in the target can be directly measured with higher accuracy than the two individual energies and over a larger energy spread of the incident beam.

2. - GENERAL CONSIDERATIONS. -

To simplify our discussion we will consider a magnetic apparatus totally achromatic with an intermediate chromatic image. This is schematically indicated in Fig. 1, which represents the median plane of the system. Axis AA' is the intersection of the plane of sym-

metry on the median plane. Axis FF' is the intersection of the final focal plane of the second magnet on the median plane.

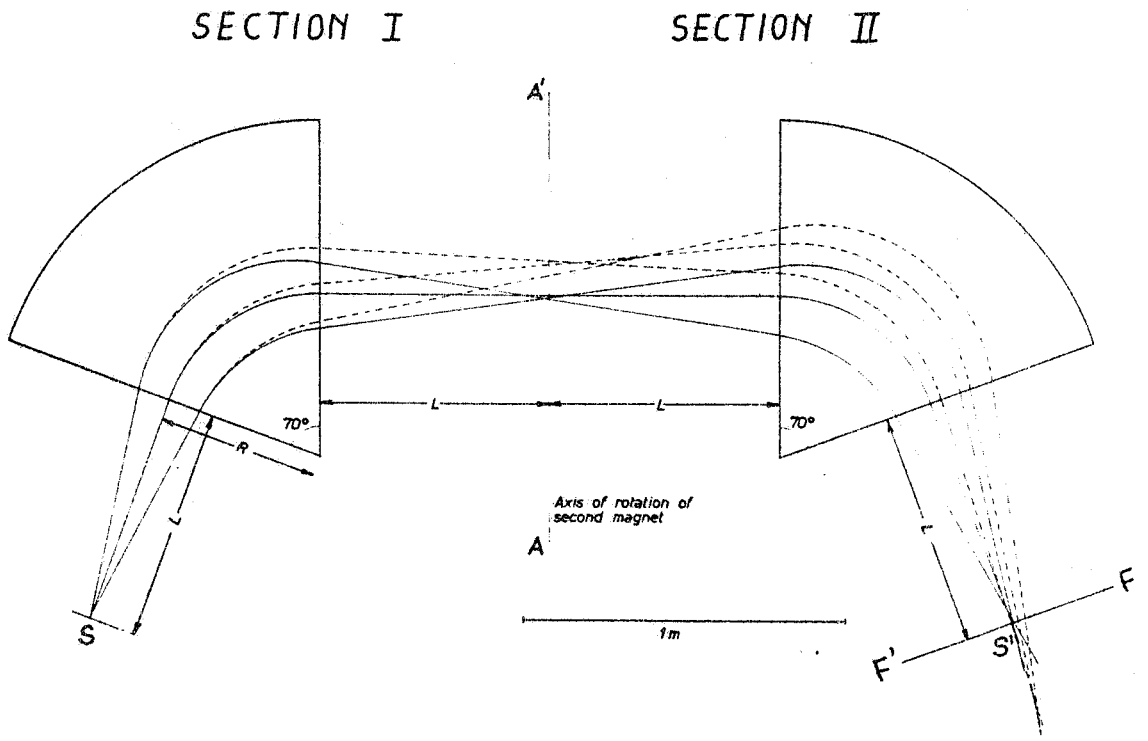

FIG. 1 - Trajectories on the median plane of the magnetic spectrometer, when the second magnet is at θ^{o} and there is no scatterer along AA'. The solid lines represent the trajectories with the central momentum and $\theta_{o} = 0, \pm 0.126$ rad. The broken lines correspond to particles with $\Delta p/p = 0.1$. The figure shows the second order aberrations of the system which produce a deterioration of the resolving power and a tilting of the focal plane. $L = 0.715$ m; $R = 0.5$ m.

In the first order approximation the particles emitted from S are analyzed by the first section, I, along the axis AA', where they are dispersed according to their momentum. The second section, II, has a dispersion equal and opposite to that of I and, therefore, brings all particles back together at S' on axis FF', irrespective of their

initial momentum. The detection counters are located on axis. If a target is inserted along axis AA', the particles, which have lost different amounts of energy in traversing this target, will focus in different points along FF'. However, the particles, which have lost the same amount of energy, will focus again in the same point to within certain approximations to be discussed later.

Let us call M_i the magnification and D_i the dispersion of the section i (i = I, II). Then, assuming a point source, the position of a particle along the axis FF' is given by:

(1) $$x_F = M_{II} D_I \gamma_I + D_{II} \gamma_{II}$$

where:

(2) $$\gamma_i = \frac{P_i - Q_i}{Q_i} \qquad i = I, II$$

is the fractional difference between the momentum P_i of the particle entering section i and the momentum of the central ray Q_i. If:

$$D_{II} = -M_{II} D_I = -D$$

(3) $$x_F = \left(\frac{P_I}{Q_I} - \frac{P_{II}}{Q_{II}}\right) D$$

and if

$$Q_I = Q_{II} = Q$$

(4) $$x_F = (P_I - P_{II}) \frac{D}{Q}$$

To perform scattering measurements at angles different from 0^o we rotate the second section around the AA' axis. As the intermediate dispersion is along this axis, the rotation does not change the achro

maticity of the entire system. This is obvious for trajectories lying on the median plane. Proper consideration must be given to the other trajectories.

3. - SYSTEM PARAMETERS. -

The performance of a simple magnetic system based on the principle of an energy loss spectrometer is reported in this article together with a detailed discussion of the basic parameters of such a system and including the second order aberrations.

The system which we have constructed and tested was originally suggested[1] to study low energy pion-nuclei scattering. It consists, Fig. 1, of two uniform field, 70^{o} bending sectors in a configuration symmetrical to first order. The basic parameters of each sector are given in Table I.

Due to the symmetry of the system, we will focus our attention upon the first section. From Table I we obtain the first order matrix element of section I:

TABLE I

Deflection angle of the central ray	$\alpha = 70^{o}$
Field gradient	$n = 0$
Radius of curvature of the central ray	$R = 0.5$ m
Width of the poles	$w = 0.22$ m
Distance of the poles	$d = 0.058$ m
Maximum magnetic field	$B_{max} = 21$ KGauss
Maximum momentum acceptance	$\Delta P/P = \pm 0.05$
Maximum solid angle	$\Delta \Omega = 0.01$ sr
Maximum angular acceptance	$\Delta \theta_o = \pm 0.126$ rad
Object and image distance from the magnet's faces	$L = 0.715$ m

(5) $\quad (x/x_o) = M_I = -1, \qquad (x/\gamma) = D_I = 1 \text{ meter}, \qquad (x/\theta_o) = 0 \text{ meters}$

where x_o and θ_o are the radial and angular displacement of an arbitrary ray measured from the central trajectory at the source S, and $\gamma = \gamma_I$ is the fractional momentum deviation of the ray from the assumed central trajectory.

3.1.- The second order aberrations and the momentum resolution of the first section.-

The energy resolution of the entire energy loss apparatus is not better than that of the first section. Therefore, we will discuss this matter in some details using the first and second order matrix notation for beam transport systems.

The displacement of a particle from the central ray in the median plane is given by[3]:

(6)
$$x = (x/x_o)x_o + (x/\theta_o)\theta_o + (x/\gamma)\gamma + (x/x_o^2)x_o^2 + (x/\theta_o^2)\theta_o^2 + \\ + (x/\gamma^2)\gamma^2 + (x/x_o\theta_o)x_o\theta_o + (x/x_o\gamma)x_o\gamma + (x/\theta_o\gamma)\theta_o\gamma$$

If the coefficients of the transport matrix (x/x_o), etc., are calculated for the transport from the object S to the image on the axis AA', then x is the displacement along AA'. These coefficients can be calculated theoretically if reasonable assumptions are introduced for the shape of the fringing field. For a sharp cut-off fringing field (SCOFF) the resulting coefficients are listed in Table II (with the symbols defined in Table I).

The second order aberrations produce a deterioration of the resolving power and a tilting of the focal plane. The tilt angle is given by[4]:

$$(7) \qquad tg\,\psi = \frac{1}{R(1-\cos\alpha)} \quad \frac{(x/\theta_o\,\gamma)}{(x/\gamma)}$$

TABLE II

$(x/x_o) = \cos\alpha - \frac{L\sin\alpha}{R}$	$(x/\theta_o) = 2L\cos\alpha + R\sin\alpha - \frac{L^2\sin\alpha}{R}$
$(x/\gamma) = L\sin\alpha + R(1-\cos\alpha)$	$(x/x_o^2) = -\frac{\sin^2\alpha}{2R}$
$(x/x_o\theta_o) = -\frac{L\sin^2\alpha}{R} + \sin\alpha\cos\alpha$	$(x/x_o\gamma) = \sin^2\alpha + \frac{L\sin\alpha}{R}$
$(x/\theta_o^2) = -\frac{R(1-\cos\alpha)}{2} + L\sin\alpha\,(\frac{1}{2}+\cos\alpha) + \frac{1}{2}R(1-\frac{L^2}{R^2})\sin^2\alpha$	
$(x/\theta_o\gamma) = L\sin\alpha\,(\sin\alpha + \frac{L}{R}) + R\sin\alpha\,(1-\cos\alpha)$	
$(x/\gamma^2) = -\frac{R\sin^2\alpha}{2} - L\sin\alpha$	

The tilting of the focal plane is particularly troublesome because scattering experiments at different angles must be performed by rotation of the second sector around axis AA'. Therefore, correct experimental results can be obtained only if the focal plane is made coincident with the symmetry plane (i.e. $\psi = 0$). The effects of the aberrations can be minimized by reducing the size of the second order coefficients appearing in equation (6).

It has been proved[5] that not all these coefficients can be simoultaneously cancelled. However, two coefficients can be made equal to zero by introducing curvatures C_1 and C_2 at the edges of the entrance and exit pole faces respectively of the magnet. Introducing C_1 and C_2 the coefficients in Table II can be rewritten as shown in Table III:

TABLE III

$$(x/x_o) = \cos\alpha - \frac{L\sin\alpha}{R}$$

$$(x/\theta_o) = 2L\cos\alpha + R\sin\alpha - \frac{L^2\sin\alpha}{R}$$

$$(x/\gamma) = L\sin\alpha + R(1-\cos\alpha)$$

$$(x/x_o^2) = \frac{\sin\alpha}{2}\left(C_1 - \frac{\sin\alpha}{R}\right) + \frac{L\cos\alpha}{2R}(C_1 + C_2\cos\alpha)$$

$$(x/x_o\theta_o) = L\sin\alpha\left(C_1 - \frac{\sin\alpha}{R}\right) + \sin\alpha\cos\alpha(1+LC_2) + \frac{L^2\cos\alpha}{R}(C_1 + C_2\cos\alpha)$$

$$(x/x_o\gamma) = \sin^2\alpha + L\left[\frac{\sin\alpha}{R} + C_2\cos\alpha\,(1-\cos\alpha)\right]$$

$$(x/\theta_o^2) = \frac{L^3\cos\alpha}{2R}(C_1 + C_2\cos\alpha) - \frac{R(1-\cos\alpha)}{2} - \frac{L\sin\alpha}{2} + \frac{L^2\sin\alpha}{2}\left(C_1 - \frac{\sin\alpha}{R}\right) +$$

$$+ L\sin\alpha\cos\alpha(1+LC_2) + \frac{R\sin^2\alpha}{2}(1+LC_2)$$

$$(x/\theta_o\gamma) = L\sin\alpha\left(\sin\alpha + \frac{L}{R}\right) + LC_2(1-\cos\alpha)(L\cos\alpha + R\sin\alpha) + R\sin\alpha(1-\cos\alpha)$$

$$(x/\gamma^2) = \frac{R}{2}\left[RC_2(1-\cos\alpha)^2 - \sin^2\alpha\right] - L\sin\alpha$$

The most serious aberration is caused by the tilting of the focal plane. The second is the sperical aberration due to the second order terms in θ_o^2. These two aberrations can be cancelled by setting:

(8) $$(x/\theta_o\gamma) = 0, \qquad (x/\theta_o^2) = 0$$

which in our case implies:

$$C_1 = 7\ m^{-1}, \qquad \varrho_1 = \frac{1}{C_1} = 0.143\ m$$

and

$$C_2 = -5.66\ m^{-1} \qquad \varrho_2 = \frac{1}{C_2} = 0.177\ m \tag{9}$$

Unfortunately these values for the radii ϱ_1 and ϱ_2 are comparable with the width, w, and the distance, d, of the magnet poles given in Table I.

Therefore the SCOFF approximation is no more valid and some corrections must be applied to take into account the shape of the fringing field. This has been done empirically by using a floating wire hodoscope to visualize the particle trajectories. We first studied the reduction of the focal plane tilting by shaping the exit poles. After some trials a good compromise was found for their mechanical profile by splitting each pole in two halves with different radii (see Fig. 2):

$$\varrho'_{m2} = -0.12 \text{ meters} \qquad \varrho''_{m2} = -0.22 \text{ meters} \tag{10}$$

The best reduction of the spherical aberration was found successively by shaping the entrance pole with the following value for the radius:

$$\varrho_{m1} = 0.091 \text{ meters} \tag{11}$$

To compare the values of the radii given by eq. (10) and (11) with the theoretical predictions of eq. (9), the formula suggested by Enge[6], modified for our actual fringing field, can be used to derive

the effective magnetic curvature of the poles:

$$C_i \simeq \frac{1}{(\varrho_{mi}+0.8d)\cos^3 \alpha_i} \qquad (i=1,2) \tag{12}$$

where d is given in Table I and α_i is the entrance (exit) angle which in our case is zero.

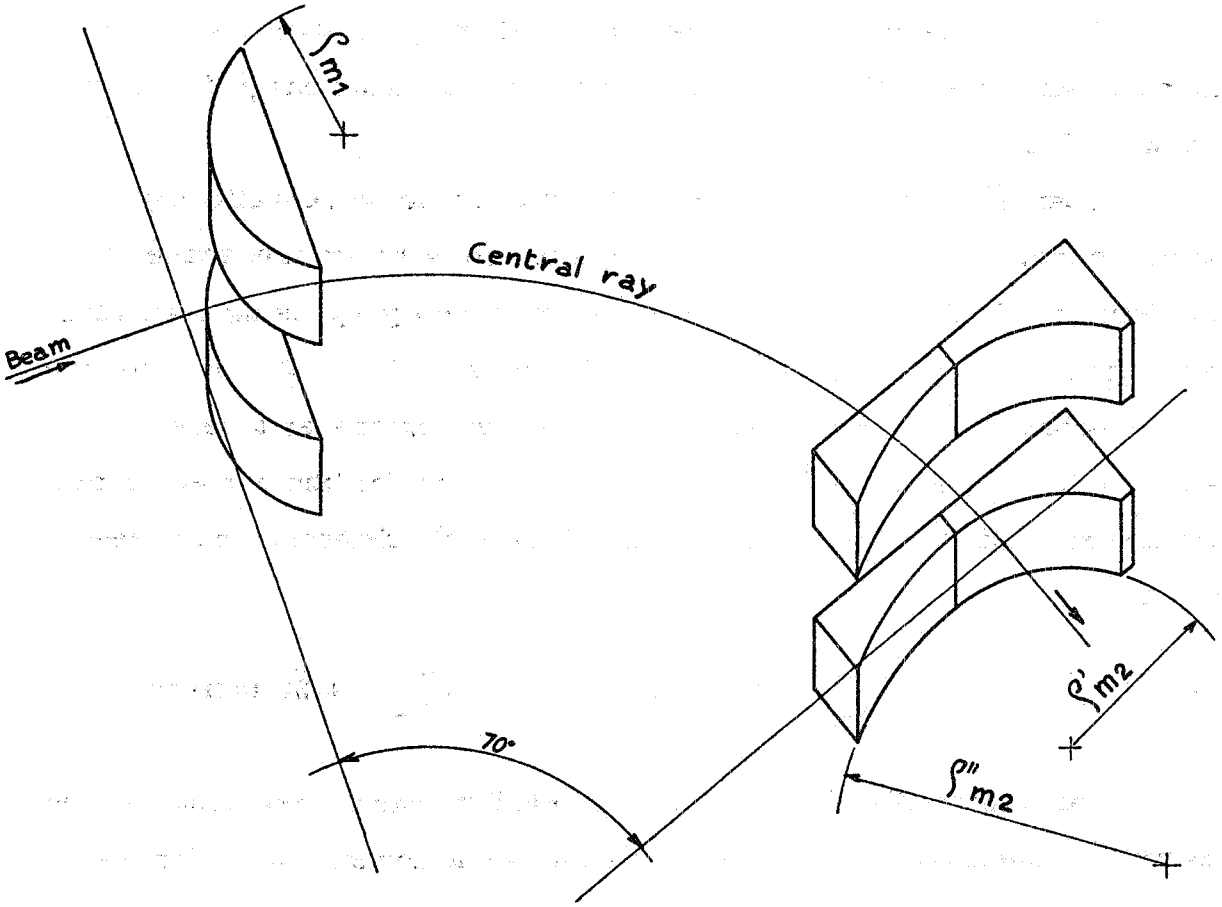

FIG. 2 - Schematics of the shaping of entrance and exit poles (first magnet). Entrance pole edge radius: ϱ_{mi} = = 0.091 m; exit pole edge radii: $|\varrho'_{m2}| = 0.12$ m, $|\varrho''_{m2}|$ = = 0.22 m.

Inserting our values for ϱ_{mi}, it follows:

$$C_1 = 7.28\ \mathrm{m}^{-1}, \qquad C_2 = -4.98\ \mathrm{m}^{-1} \tag{13}$$

where for C_2 we have taken the average of the values obtained with the radii quoted in eq. (10). These results are in good agreement with the theoretical ones of eq. (9).

In Table IV we listed the second order coefficients of the transport matrix calculated with no pole shaping (column one), with the curvatures given in eq. (9) (column two) and with those given in eq. (13). (Units are m, rad).

TABLE IV

	1	2	3	4
	One Section	One Section	One Section	Two Sections
$C_1(m^{-1})$	0	+7.00	+7.28	+ 7.28
$C_2(m^{-1})$	0	- 5.66	- 4.98	- 4.98
(x/x_o^2)	- 0.88	+3.64	+3.90	+10.16
$(x/x_o\theta_o)$	- 0.94	+4.23	+4.76	+ 1.32
$(x/x_o\gamma)$	+2.23	+1.32	+1.43	- 25.73
(x/θ_o^2)	- 0.50	0	+0.34	+ 0.012
$(x/\theta_o\gamma)$	+1.90	0	+0.23	- 5.89
(x/γ^2)	- 0.89	- 1.33	- 1.28	+10.33

Let us now calculate the momentum resolving power δ_A^S(FWHM) of the single section.

Inserting in eq. (6) the numerical values of the coefficients as given in Table IV, column 3, we obtain for $\gamma = 0$,

(14) $$x = -x_o + 0.34\,\theta_o^2 + 4.76\,x_o\,\theta_o$$

where x_o and θ_o have approximately rectangular probability distributions with the respective half width given by:

(15) $$x_o^{max} = 0.005 \text{ m} \qquad \text{and} \qquad \theta_o^{max} = 0.126 \text{ rad.}$$

The FWHM of this distribution has been evaluated with a Monte Carlo calculation and the final result for the momentum resolution is

(16) $$\delta_A^S(\text{FWHM}) = 8.8 \text{ mm} = 0.88\%$$

according to the dispersion of the single magnet as given in equation (5).

4. - MEASUREMENTS WITH THE PION BEAM. -

The measurements have been carried out with the low energy pion beam of the Frascati National Laboratories with the magnets set at 0^o facing each other . Multiple Coulomb scattering in air, Helium and thin windows was the only source of perturbation on the particle trajectories. These effects, however, will be neglected at first and introduced at a later stage.

4.1. - The Second Order Aberrations of the Two Magnets System. -

In this configuration a careful discussion of the second order aberrations of the entire magnetic system must be made to understand the experimental results shown in Fig. 4.

The first and second order matrix elements for the entire system must be calculated since the particles move directly from

the first section to the second one without appreciable perturbation of their momentum vector. The first order matrix elements are strictly determined by the geometry of the system. Those of the second order still include some free parameters such as the curvatures (C_1^{II} and C_2^{II}) of the pole faces of the second magnet. These curvatures could be adjusted to reduce the overall effect of the second order aberrations. However the momentum resolution at 0^o is not the same as that under actual scattering conditions, with the second magnet at an angle different from 0^o. In fact the angle of the particles at the intermediate image on the axis AA' is altered during the scattering process and therefore the angle-momentum and angle-position correlations are lost on this axis.

The first measurements have been made with the curvatures of the poles of the second magnet equal to those of the first one. In this configuration the second magnet is identical to the first one but the entire configuration is not symmetrical to the second order.

With the following values for the curvatures:

$$C_1^I = C_1^{II} = 7.28 \text{ m}^{-1}, \qquad C_2^I = C_2^{II} = -4.98 \text{ m}^{-1} \tag{17}$$

the theoretical values of the second order matrix elements are indicated in column four of Table IV.

The phase space of the particles transmitted by the two magnets system at zero degrees is given by the following considerations.

The pole width of the first magnet limits the angular acceptance of the system:

$$|\theta_o|_{max} = 0.126 \text{ rad} \tag{18}$$

The energy defining slits positioned along AA' define the momentum

acceptance. They were adjusted in such a way that:

$$|\gamma|_{max} = 0.05 \tag{19}$$

A slit placed halfway of the second magnet, 0.088 m wide, sets an upper limit to the radial displacement x. Inserting in eq. (6) the transport coefficients evaluated between the source and the slit's position, with the curvatures given in eq. (17), gives the following constraint:

$$\begin{aligned} &|1.73\,\gamma - 0.87\theta_o - 2.4x_o + 16.7x_o^2 + 12.7x_o\theta_o - 15.5x_o\,\gamma + 0.044\theta_o^2 - \\ &-6.3\theta_o\,\gamma + 3.8\,\gamma^2| \leqq 0.044 \text{ m} \end{aligned} \tag{20}$$

Therefore, the momentum resolution of our entire system can be obtained from the threefold distribution of the variable

$$x = 0.01\,\theta_o^2 - 5.89\,\theta_o\gamma + 10.33\,\gamma^2 + x_o + 10.16\,x_o^2 + 1.32\,x_o\theta_o - 25.73\,x_o\gamma \tag{21}$$

with the boundary conditions set by equations (18)(19)(20). The FWHM of this distribution has been evaluated with a Monte Carlo calculation and the final result is:

$$\delta_A^T(\text{FWHM}) = 11.7 \text{ mm} \tag{22}$$

where δ_A^T is the contribution of the aberrations to the momentum resolution of the two magnets system.

4.2.- Multiple Coulomb scattering and the momentum resolution.-

Multiple Coulomb scattering changes slightly the direction of the particles during their flight from the source to the detection counter. This affects the momentum resolution of the system in a way that can be easily calculated by using the first order matrix notation.

Let σ_x^2 be the mean square displacement of a particle along FF' due to the multiple Coulomb scattering along its path. Then:

$$\sigma_x^2 = \int_S^{S'} M_{12}^2(t)\, d\,\sigma_\theta^2(t) \tag{23}$$

where M_{12} is the matrix element (x/θ_o) for the transport of a particle from the arbitrary point to the counter along FF' and $\sigma_\theta^2(t)$ is the mean square angle of multiple scattering in the thickness t. If the system has an intermediate image point, the matrix element M_{12} can be calculated from the arbitrary point to the intermediate image and the result is multiplied by the magnification $\left[M_{11}=(x/x_o)\right]$ from that image to the detector.

Numerical calculations for the multiple scattering have been carried out following the theory of Nigam, Sundaresan and Wu[7] (NSW) in the approximate formulation given by Marion and Zimmerman[8] for medium energy particles and moderate thickness materials. The parameters of this theory are χ_c and B, where

$$\chi_c = 0.1569\, \frac{Z(Z+1)z^2 t}{A(pv)^2} \tag{24}$$

and B is defined through the following relations

$$B - \ln B = B_o \tag{25}$$

$$B_o = \ln\left[2730(Z+1)Z^{1/3} z^2 t/A\,\beta^2\right] - 0.1544 \tag{26}$$

z and Z are the atomic number of the incident particle and the scatterer respectively, A the atomic weight of the scatterer, t the thickness of the scattering foil (gr/cm^2), p.v the momentum velocity product of the incident particle in MeV, $\beta = v/c$.

Since most of the scattering in restricted to forward angles where the shapes of the angular distributions are approximately Gaussian, in the hypothesis of reference[8] it is sufficient to represent the angular distribution by a Gaussian function $F(\zeta)$ which is chosen to have the same width of the angular distribution at the 1/e point. By defining

(27) $$\zeta = \theta / \chi_c B^{1/2}$$

the distribution is given by

(28) $$F(\zeta) \propto \exp(-\zeta^2 / \zeta_w^2)$$

where the width parameter ζ_w is related to the angle at which the angular distribution has fallen to 1/e of its value at $\zeta = 0$. The theory is valid for $4 \leq B \leq 15$.

In order to perform the integration indicated in (23), we have used an approximate analytical expression for $\sigma_\theta(t)$. A discrete set of σ_θ values has been calculated in a wide range of the thickness τ ($\tau = t/t_o$, where t_o is the radiation length) according to the NSW theory. The (σ_θ, τ) data points have been fitted with a function of the type

(29) $$\sigma_\theta(\tau) = \frac{15}{p\beta} \sqrt{\tau} (a + b\,\tau^c)$$

The parameters a, b and c are plotted versus the pion energy in Fig. 3.

Three special cases of multiple scattering must be discussed here:

1) The scatterer is concentrated at a distance L from the image point. In this case

$$M_{12} = L$$

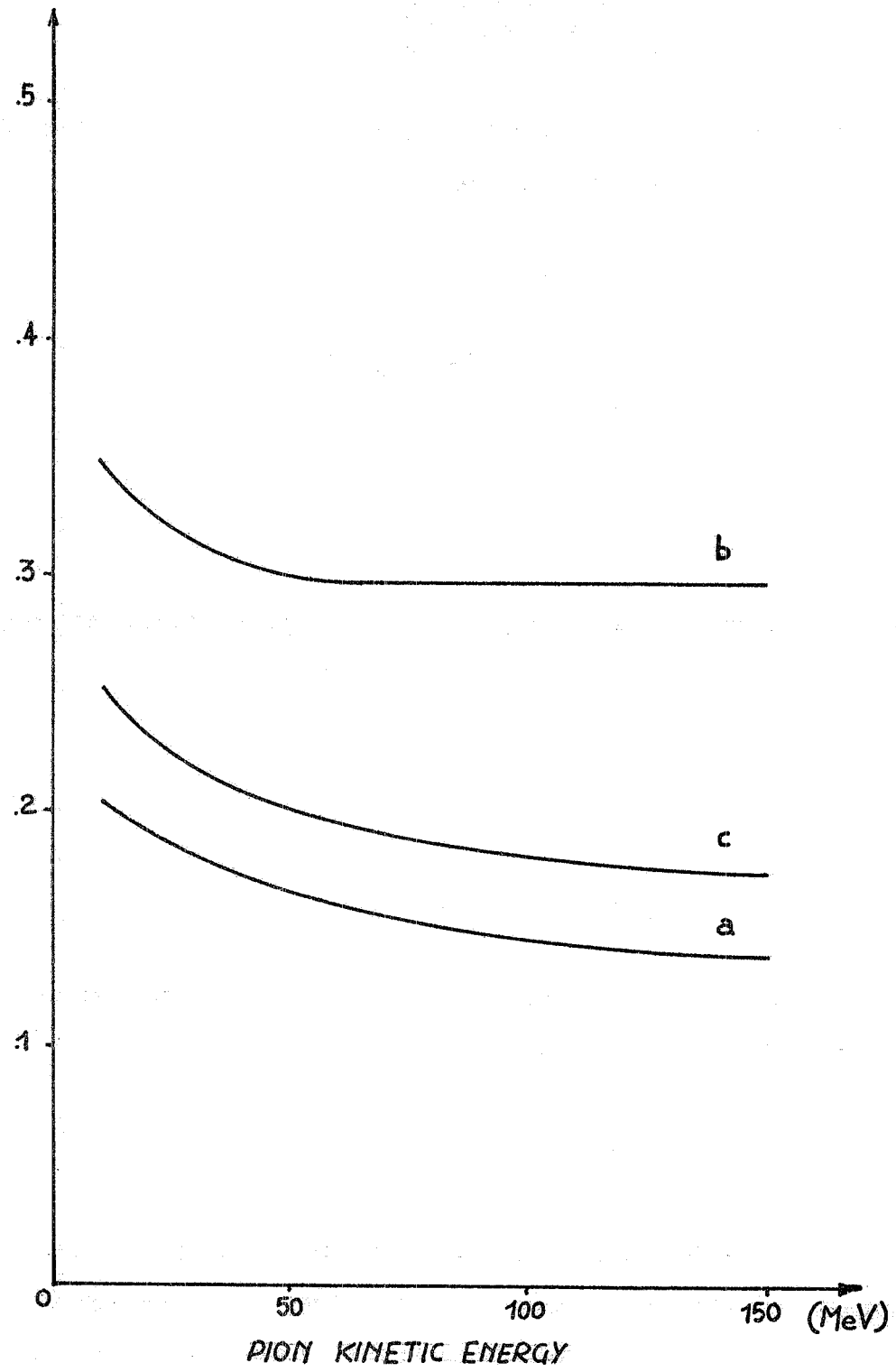

FIG. 3 - The adimensional best-fit parameters a, b, c of eq. (29) plotted vs. the pion kinetic energy.

(30) $$\sigma_x^2 = \int L^2 \, d\,\sigma_\theta^2 = L^2 \, \sigma_\theta^2$$

2) The scatterer is distributed before an image point starting at a distance L in a field free region. In this case

$$M_{12} = t$$

(31) $$\sigma_x^2 = \int_o^L t^2 \, d\,\sigma_\theta^2(t) = t_o^2 \int_o^{\tau_o} \tau^2 \, d\,\sigma_\theta^2(t)$$

where

(32) $$\tau_o = L/t_o$$

The resulting mean square displacement is given, according to (34), by

(33) $$\sigma_x^2 = \sigma_{x,RG}^2 \, H(\tau_o)$$

where

(34) $$\sigma_{x,RG}^2 = \left(\frac{15}{p\beta}\right)^2 \frac{1}{t_o} \, \frac{L^3}{3}$$

is the mean square displacement calculated with the approximate formula of Rossi and Greisen[9] and

(35) $$H(\tau_o) = a^2 + \frac{6\,ab(1+c)}{3+c} \, \tau_o^c + \frac{3\,b^2(1+2c)}{2c+3} \, \tau_o^{2c}$$

3) The scatterer is distributed in a uniform magnetic field bending sector of angle α and radius of curvature R. The magnet is separated from an image point by a field free empty space of length L. In this case

(36) $$M_{12} = L\cos\varphi + R\,\mathrm{sen}\,\varphi \qquad (0 \leq \varphi \leq \alpha)$$

(37) $$\sigma_x^2 = \int_o^a (L\cos\varphi + R\sin\varphi)^2 \, d\sigma_\theta^2(t)$$

which now gives:

(38) $$\sigma_x^2 = \left(\frac{15}{p\beta}\right)^2 \int_o^a P(\tau)(L\cos\varphi + R\sin\varphi)^2 \, d\tau$$

where

(39) $$P(\tau) = a^2 + 2ab(1+c)x^c + b^2(1+2c)x^{2c}$$

But

(40) $$d\tau = \frac{R\,d\varphi}{t_o}$$

and $P(\tau)$ is a slowly varying function in the interval

(41) $$0 \leq \tau \leq \frac{R\alpha}{t_o}$$

so we can rewrite equation (38)

(42) $$\sigma_x^2 = \left(\frac{15}{p\beta}\right)^2 \frac{R}{t_o} \bar{P}(\tau)\left[\frac{\alpha}{2}(L^2+R^2) + LR\sin^2\alpha + \frac{1}{4}(L^2-R^2)\sin 2\alpha\right]$$

where $\bar{P}(\tau)$ is a mean value of the polynomial $P(\tau)$ in the above considered interval.

In Table V we report materials, thicknesses and distances encountered by the pions in our experimental apparatus.

4.3. - Results. -

The contribution of multiple Coulomb scattering to the momentum resolution of the two magnets system is given by

(43) $$\delta_{MS}(FWHM) = 2\sqrt{2\ln 2} \cdot \sigma_x$$

TABLE V

Type	Thickness (cm)	Distance (cm)
Mylar window	0.0178	52
Air before target	52	52
Air after target	60	60
Mylar window	0.0045	60
Helium	R = 50 cm	$\alpha = 70^{o}$
Helium	31.5	31.5
Mylar window	0.0045	40
Air before detector	40	40

The numerical values of the three separate contributions of multiple scattering to the momentum resolution are listed in Table VI together with the total effect, δ^{T}_{MS}, at various energies.

The total momentum resolution of the system is obtained combining quadratically the contribution of the aberrations, δ^{T}_{A} (Table VI, column six), with δ^{T}_{MS}. The result, $\delta^{theor.}_{tot}$, is indicated in column seven and compared in Fig. 4 with the experimental results obtained for positive and negative pions.

TABLE VI

T_π (MeV)	δ^{c}_{MS} (mm)	δ^{d}_{MS} (mm)	δ^{m}_{MS} (mm)	δ^{T}_{MS} (mm)	δ^{T}_{A} (mm)	$\delta^{theor.}_{tot}$ (mm)	$\delta^{exp}_{\pi^-}$ (mm)	$\delta^{exp}_{\pi^+}$ (mm)
30	4.28	3.76	0.51	5.72	11.70	13.02		15.07±1.37
50	2.57	2.30	0.31	3.47	11.70	12.20	13.70±1.37	
80	1.65	1.51	0.21	2.24	11.70	11.91	10.96±1.37	12.33±1.37
100	1.34	1.23	0.16	1.83	11.70	11.84	9.59±1.37	10.96±1.37
120	1.14	1.04	0.14	1.55	11.70	11.80		10.96±1.37
130	1.06	0.97	0.13	1.44	11.70	11.79	10.96±1.37	9.59±1.37
150	0.93	0.86	0.11	1.28	11.70	11.77	9.59±1.37	9.59±1.37

The various full width half maximum resolutions vs. the pion kinetic energy.

δ^{c}_{MS} is the contribution due to concentrated scatterers

δ^{d}_{MS} is the contribution due to distributed scatterers

δ^{m}_{MS} is the contribution due to the scatterer distributed in a magnetic field bending sector.

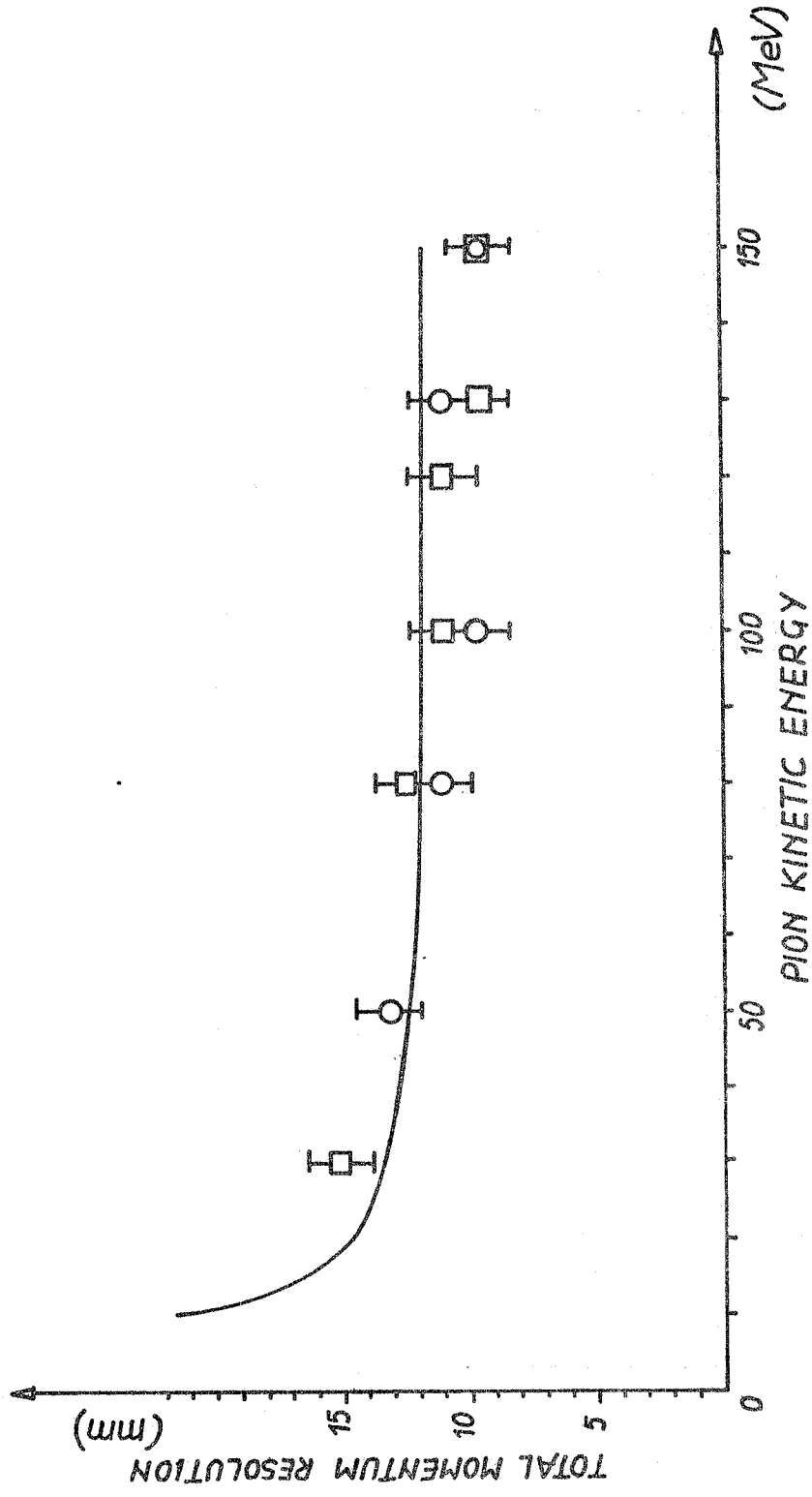

FIG. 4 - Total momentum resolution of the energy loss spectrometer. □ = $\delta^{exp}_{\pi^+}$ (experimental); O = $\delta^{exp}_{\pi^-}$ (experimental); the full line represents the theoretical resolution $\delta^{theor.}_{tot}$ (see Table VI, column 9, 8 and 7).

REFERENCES. -

(1) - C. Schaerf and R. Scrimaglio, Nuclear Instr. and Meth. 30, 359 (1964).

(2) - J. F. Streib, HELPL Report n. 104, Stanford (1960); K. L. Brown, SLAC Report n. 75, Stanford (1971); K. L. Brown, Adv. Particles Phys. 1, 71 (1967).

(3) - K. L. Brown, R. Belbeoch and P. Bounin, Rev. Sci. Instr. 35, 481 (1964); R. H. Helm, SLAC Report n. 24, Stanford (1963); K. L. Brown Proc. Fifth Intern. Conf. on High Energy Accelerators, Frascati (1965), pp. 507-513; S. Kowalski, Lectures at the Advanced Institute on Electron Scattering and Nuclear Structure, Santa Margherita di Pula, (1970).

(4) - P. Bounin, Rev. Sci. Instr. 38, 1305 (1967).

(5) - M. Donnetti and G. Sanna, Rev. Sci. Instr. 42, 1339 (1971).

(6) - A. Enge, Deflecting Magnets in Focusing of Charged Particles, edited by A. Septier (Academic Press, New York & London 1967) Vol. II.

(7) - B. P. Nigam, M. K. Sundaresan and T. Y. Wu, Phys. Rev. 115, 491 (1959).

(8) - J. B. Marion and B. A. Zimmerman, Nuclear Instr. and Meth. 51, 93 (1967).

(9) - B. Rossi, High Energy Particles (Prentice-Hall Inc., Englewood Cliffs (N. J.) 1952).